BIOCHEMISTRY
including biophysical chemistry & molecular biology

ARTICLE

pubs.acs.org/biochemistry

Identification of Two Imidazole Binding Sites and Key Residues for Substrate Specificity in Human Primary Amine Oxidase AOC3

Heli Elovaara,[†,‡] Heidi Kidron,[§,▽] Vimal Parkash,[§] Yvonne Nymalm,[§,●] Eva Bligt,[§] Pauli Ollikka,[∥] David J. Smith,[∥] Marjo Pihlavisto,[∥] Marko Salmi,[‡,⊥] Sirpa Jalkanen,[†,‡] and Tiina A. Salminen*[,§]

[†]Medicity Research Laboratory, University of Turku, FI-20520 Turku, Finland

[‡]National Institute for Health and Welfare, FI-20520 Turku, Finland

[§]Structural Bioinformatics Laboratory, Department of Biosciences, Åbo Akademi University, FI-20520 Turku, Finland

[∥]BioTie Therapies Corporation, FI-20520 Turku, Finland

[⊥]Department of Medical Biochemistry and Genetics, University of Turku, FI-20520 Turku, Finland

Supporting Information

ABSTRACT: Human membrane primary amine oxidase (hAOC3; also known as vascular adhesion protein-1, VAP-1) is expressed upon inflammation in most tissues, where its enzymatic activity plays a crucial role in leukocyte trafficking. We have determined two new structures of a soluble, proteolytically cleaved form of hAOC3 (sAOC3), which was extracted from human plasma. In the 2.6 Å sAOC3 structure, an imidazole molecule is hydrogen bonded to the topaquinone (TPQ) cofactor, which is in an inactive on-copper conformation, while in the 2.95 Å structure, an imidazole molecule is covalently bound to the active off-copper conformation of TPQ. A second imidazole bound by Tyr394 and Thr212 was identified in the substrate channel. We furthermore demonstrated that imidazole has an inhibitory role at high concentrations used in crystallization. A triple mutant (Met211Val/Tyr394Asn/Leu469Gly) of hAOC3 was previously reported to change substrate preferences toward those of hAOC2, another human copper-containing monoamine oxidase. We now mutated these three residues and Thr212 individually to study their distinct role in the substrate specificity of hAOC3. Using enzyme activity assays, the effect of the four single mutations was tested with four different substrates (methylamine, benzylamine, 2-phenylethylamine, and *p*-tyramine), and their binding modes were predicted by docking studies. As a result, Met211 and Leu469 were shown to be key residues for substrate specificity. The native structures of sAOC3 and the mutational data presented in this study will aid the design of hAOC3 specific inhibitors.

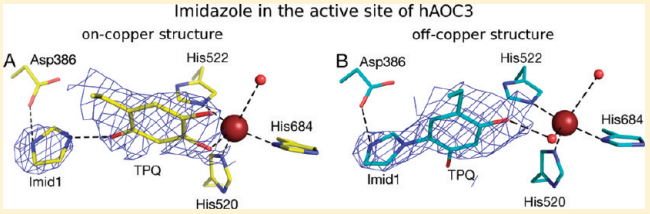

Human membrane primary amine oxidase (hAOC3, also called vascular adhesion protein-1,[1] VAP-1, EC 1.4.3.21) belongs to the copper-containing amine oxidase/semicarbazide-sensitive amine oxidase (CAO/SSAO) family. Dimeric CAOs are found in mammals, plants, and bacteria.[2] In mammals, the CAOs are involved in, for example, signaling, adhesion, and apoptosis (for reviews, see refs 3−5). CAOs catalyze the oxidative deamination of primary amines to aldehydes in a reaction in which hydrogen peroxide and ammonia are also produced. The catalytic reaction mechanism has been thoroughly studied in bacteria and yeast (Scheme 1) (for a review, see ref 6). First, the amine substrate binds to the post-translationally modified tyrosine cofactor topaquinone (TPQ) of an oxidized enzyme forming a substrate Schiff base. Second, a proton from the α-carbon of the substrate is abstracted by the general base (Asp386 in hAOC3), and the product Schiff base is then hydrolyzed, releasing the aldehyde product after which the enzyme is reduced. To reactivate the enzyme, it is oxidized by molecular oxygen while hydrogen peroxide and ammonia are released.

Depending on the nature of their substrates, CAOs can be further classified as mono- or diamine oxidases. In humans, three CAOs (hAOC1−3) have been characterized. hAOC1 is a diamine oxidase, which is expressed in, for example, placenta, kidney, gut, and lung.[7] hAOC1 degrades exogenous histamine, and the decreased levels of the protein correlate with histamine intolerance.[8] hAOC2 and hAOC3 are monoamine oxidases. hAOC2 is a retinal amine oxidase that has been detected in other tissues as well, but its physiological role is unknown.[9,10] hAOC3 is primarily expressed in endothelial cells, smooth muscle cells, and adipocytes.[11,12] In adipocytes, hAOC3 acts in glucose metabolism.[13] On the endothelial cell surface, hAOC3 expression is upregulated upon inflammation,[11,14] and it has an essential role in extravasation of leukocytes from the blood into tissues.[15−20]

The CAO activity in human serum originates from proteolytically cleaved membrane-bound hAOC3, which is released into

Received: January 24, 2011
Revised: May 17, 2011
Published: May 18, 2011

Scheme 1. Mechanism for the Reductive Half-Reaction of CAOs

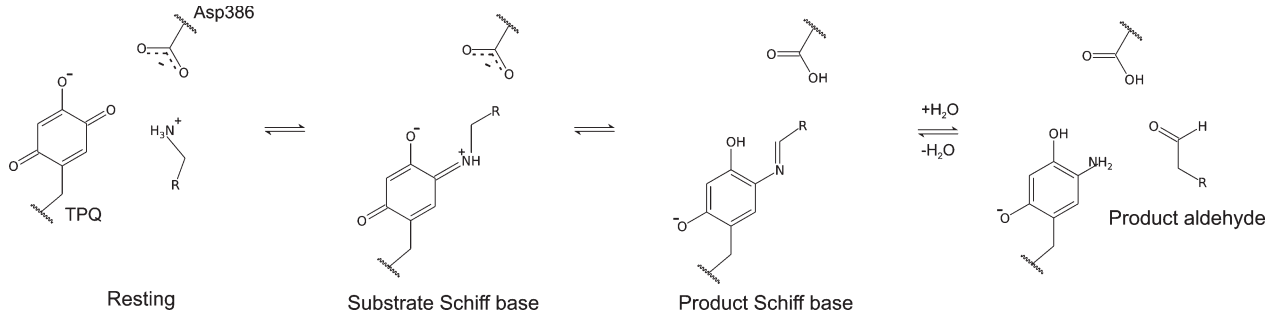

plasma in a soluble form and thus called sAOC3.[21−23] Healthy humans have a low level of sAOC3 activity in serum, but elevated sAOC3 levels have been reported under different inflammatory conditions, e.g., diabetes, congestive heart failure, and liver disorders in which the diseased organ seems to be the main source of sAOC3.[13,24] Many other mammals, including cattle and pig, have a much higher level of serum CAO activity, which originates from a secreted CAO that is encoded by the *AOC4* gene.[25] The enzymatic activity studies of mammalian CAOs have been mainly conducted with the bovine serum amine oxidase (BSAO) encoded by the *AOC4* gene. The *AOC4* gene in humans, however, appears to be a pseudogene.[25] Interestingly, BSAO and hAOC3 were recently shown to have different kinetic behavior with respect to the most commonly used amine oxidase substrate, benzylamine; a two-site binding of benzylamine could be detected for BSAO, but it could not be demonstrated for hAOC3.[26] Therefore, one needs to be careful when results obtained with BSAO are generalized to hAOC3.

The X-ray structures of hAOC3 and hAOC1 have been determined.[27−30] They are both homodimers with monomer sizes of 94 and 85−90 kDa, respectively,[7,31] and they share the typical three-domain (D2, D3, and D4) amine oxidase fold, with a level of sequence identity of 38%.[29] The molecular structure of hAOC2 is not known; however, hAOC2 and hAOC3 share a level of sequence identity of 68%, and their overall structures are predicted to be very similar.[10] The catalytic residues in the active sites of CAOs are well-conserved, including TPQ, the catalytic aspartate, and the three histidines binding the copper ion. In the published hAOC3 structures, TPQ is in an inactive on-copper[27] or active off-copper conformation.[28,30] The two active sites are buried in the D4 domains and accessible only via the substrate channels, which differ in hAOCs.

The substrate specificity differences among the three human CAOs are likely to arise from a combination of amino acid substitutions and differences in the dimensions of the substrate channel and the active site cavity. In hAOC1, the entrance to the substrate channel is narrower than in hAOC3, and there are nonconserved residues in the channel wall that can interact with substrates or inhibitors.[29] The active site cavity in the hAOC3 structure is much smaller than that in the hAOC2 model.[10] We have shown that the substrate specificity of hAOC3 can be changed toward the substrate preferences of hAOC2 via mutation of three nonconserved residues in the active site cavity of hAOC3 to the corresponding ones in hAOC2 (a Met211Val/Tyr394Asn/Leu469Gly triple mutant).[10]

As the native structure of human AOC3 and identification of functionally important residues are needed for designing specific inhibitors that are better than those currently available, we determined two structures of sAOC3 in this work. Moreover, we investigated the individual roles of four nonconserved active site residues (Met211, Thr212, Tyr394, and Leu469) in the catalytic activity of hAOC3 by site-directed mutagenesis, enzymatic assays, and computational docking studies. The results obtained will provide a structural starting point for inhibitor design.

EXPERIMENTAL PROCEDURES

Reagents. All the reagents were from Sigma-Aldrich unless otherwise indicated.

Crystallization, Data Collection, and Structure Determination. The soluble form of AOC3 (sAOC3, amino acids 27−763) was extracted and purified from human serum by BioTie Therapies Corp. The human serum sample was first prefiltered, concentrated, and purified as described previously for recombinant hAOC3,[32] and finally dialyzed against 10 mM potassium phosphate (pH 7.2). The protein was concentrated to approximately 1.0 mg/mL and crystallized as described previously for recombinant hAOC3.[32,33] Briefly, hexagonal crystals appeared after a week in hanging drops containing 2 μL of well solution [0.7 M potassium/sodium tartrate, 100 mM imidazole (pH 7.4), and 200 mM NaCl] and 2 μL of protein solution at room temperature. For data collection, the crystals were dipped in 0.6 M potassium/sodium tartrate, 100 mM imidazole (pH 7.4), 200 mM NaCl, and 2 M sodium formate and flash-frozen using liquid nitrogen. X-ray analysis and data collection were conducted using synchrotron radiation at MAX-lab (Lund, Sweden) and ESRF (Grenoble, France) (Table 1). The data were processed with XDS[34] in space group $P6_522$. Phaser[35] within the CCP4i program suite[36] was used to determine the structures with molecular replacement using phase information from the determined recombinant hAOC3 structure [Protein Data Bank (PDB) entry 1US1].[27] One biological unit, a dimer, was located in the asymmetric unit of both structures. The model was first refined as a rigid body with REFMAC5.[37] The models were rebuilt using COOT[38] followed by multiple rounds of restrained refinement using PHENIX.[39] The molecular replacement solution after refinement of the 2.95 Å structure in the on-copper conformation had negative and positive $F_o - F_c$ density in the topaquinone regions in both monomers (Figure S1 of the Supporting Information). It suggested that the TPQ should be built in the off-copper conformation. When the TPQ was changed to the off-copper conformation (Figure S2 of the Supporting Information), the negative and positive $F_o - F_c$ density disappeared. Omit maps[40] calculated in these doubtful regions confirmed the off-copper state of the 2.95 Å structure.

Table 1. Summary of Data Collection and Structure Refinement Statistics

	on-copper	off-copper
	Data Collection[a]	
beamline	I711 (MAX-lab, Lund, Sweden)	BM14 (ESRF, Grenoble, France)
space group	$P6_522$	$P6_522$
unit cell dimensions	$a = b = 225.8$ Å, $c = 217.0$ Å	$a = b = 225.8$ Å, $c = 218.7$ Å
	$\alpha = \beta = 90°$, $\gamma = 120°$	$\alpha = \beta = 90°$, $\gamma = 120°$
resolution limits (Å)	29.93−2.60 (2.70−2.60)	38.50−2.95 (3.05−2.95)
no. of observed reflections	1181064 (126033)	503881 (46698)
no. of unique reflections	99745 (10523)	69215 (6498)
wavelength (Å)	0.91	0.97
Matthews coefficient (Å^3/Da)	2.24	2.24
solvent content (%)	45	45
unit cell volume (Å^3)	9577124	9656668
no. of monomers per asymmetric unit	2	2
completeness (%)	99.9 (100.0)	99.8 (100.0)
redundancy	11.8 (11.9)	7.3 (7.1)
R_{sym} (%)	12.3 (51.7)	13.6 (48.1)
R_{meas} (%)	12.9 (54.0)	14.6 (51.8)
$R_{mrgd\text{-}F}$ (%)	8.8 (25.9)	11.9 (38.1)
average I/σ	17.5 (5.1)	13.9 (4.3)
Wilson B factor	36.0	35.6
	Structure Refinement[a]	
PDB entry	2Y73	2Y74
resolution range (Å)	20.00−2.60 (2.69−2.60)	38.20−2.95 (3.05−2.95)
no. of reflections	99551	69194
R_{cryst} (%)	17.5	17.9
R_{free} (%)	21.3	21.4
no. of amino acids	1406	1394
no. of water molecules	346	129
no. of sugar molecules	14	14
average B factor for all atoms (Å^2)	37.3	34.0
Ramachandran plot (%)		
most favored	94.6	95.2
additional allowed	4.8	4.1
disallowed regions	0.6	0.7

[a] Values in parentheses represent those for the highest-resolution bin.

The stereochemical qualities of the structures were assessed with PROCHECK[41] and WHATIF,[42] and the structure determination statistics are presented in Table 1.

Absorbance Spectroscopy of sAOC3. The absorption spectrum of sAOC3 [1 mg/mL in 20 mM phosphate-buffered saline and 0.03% Triton X-100 (pH 7.4)] from 300 to 700 nm was measured (Amersham Ultrospec 3300 pro spectrophotometer). Two samples of sAOC3, one with 100 mM imidazole and another without imidazole (control), were prepared as follows. Either 8 μL of 1 M imidazole or 8 μL of 10 mM KPO_4 (pH 7.6) was added to the 72 μL sAOC3 sample. The samples were incubated for 30 min at room temperature (RT), and absorption spectra of the samples were recorded. *p*-Nitrophenylhydrazine (*p*-NPH) was added to a final concentration of 50 μM, and the samples were incubated for 30 min at RT. After incubation, 50 μL of the samples was dialyzed against 100 mL of 10 mM KPO_4 (pH 7.6) with and without imidazole for 3 h. After dialysis, 30 μL of 10 mM KPO_4 was added to the samples and the absorption spectra were recorded.

DNA and Mutants. hAOC3 has been cloned previously.[31] The mutations were introduced by a polymerase chain reaction (PCR) using Phusion DNA polymerase (Finnzymes, Helsinki, Finland) according to a basic protocol described by the manufacturer (the sequences of the primers are available on request). The PCR products were purified from an agarose gel, self-ligated using T4 DNA ligase (New England Biolabs), and electroporated into *Escherichia coli* DH5α. The success of the PCRs was confirmed by sequencing the whole *hAOC3* gene.

Cells and Transfections. Previously reported stable Chinese hamster ovary cell lines for hAOC3 (CHO-VAP-1) and mock control (CHO-pcDNA3.1) were used to study the effect of imidazole on hAOC3 activity.[31] The cells were grown in F-12K Nutrient Mixture (Gibco) supplemented with 10% fetal calf serum, 100 units/mL penicillin, and 100 mg/mL streptomycin. Confluent cells were collected by a short trypsin treatment and lysed in 10 mM Tris-HCl (pH 7.2), 1.5 mM $MgCl_2$, and 0.1% nonident P-40 (lysis buffer) for 1−2 h at 4 °C using end-over-end rotation. The supernatants were collected by centrifugation

(30 min at 4 °C and 12000*g*) and stored at −20 °C. Total protein concentrations were assayed using a modified Lowry's method and the DC Protein Assay (Bio-Rad), and bovine serum albumin (BSA) was used as a reference.[43,44] The recombinant hAOC3 and mutant proteins for the activity assays were expressed in Hamster embryonic kidney (HEK) 293 EBNA cells. The cells were cultured in Dulbecco's modified Eagle's medium supplemented with 10% fetal calf serum, 2 mM L-glutamine, 100 units/mL penicillin, 100 mg/mL streptomycin, and 0.25 mg/mL G418 sulfate. For transfection, the cells were plated on a six-well plate ($5-6 \times 10^5$ cells/well) and cultured overnight at 37 °C in 5% CO_2. The next day, the transfection was performed using 3−8 μL of Fugene HD transfection reagent (Roche Applied Science, Indianapolis, IN) and 2 μg of DNA per well. The cells were collected and lysed after 24 h as described above. The success of the transfection was assayed by immunofluorescence staining using fluorescent isothiocyanate (FITC)-conjugated anti-hAOC3 monoclonal antibody TK-8-14 (2 μg/mL).[22] An equal amount of 3G6-FITC against chicken T cells was used as a negative control. The measurements were taken with Fluorescence Activated Cell Sorter (FACSCalibur) and Cellquest.

Imidazole and hAOC3 Activity. The role of imidazole in hAOC3 activity was studied as described previously.[45,46] In brief, 20 μg of CHO-VAP-1 lysates was incubated at 37 °C in 25 mM HEPES (pH 7.4), 150 mM NaCl, and 0.1−100 mM imidazole. After 20 min, a substrate solution [2 mM [7-^{14}C]benzylamine (Amersham Pharmacia, 54 mCi/mmol) with 1 μM cold benzylamine] was added. The reactions were stopped after 2 h via addition of 100 μL of 2 M citric acid and 3.5 mL of 1.6 mM 2,5-diphenyloxazole in toluene. The aqueous phases were then frozen at −40 °C, after which the organic phases were poured into clean scintillation vials for counting. The counting was done with a WALLAC-1409 liquid scintillation counter (Wallac Oy, Turku, Finland). Every concentration was determined in triplicate. The background activity was measured in the presence of 1 mM semicarbazide. The mock (CHO-pcDNA3.1) lysate was used as a control. The controls were conducted as duplicates. The activities are presented as relative activity (100% refers to the activity without imidazole; the background activities are always subtracted). The data were fitted to a one-site competition model using GraphPad (GraphPad Software Inc., La Jolla, CA).

Enzyme Activity Assays. The hAOC3 activity was measured from the transiently transfected cell lysates using a hydrogen peroxide-sensitive Amplex Red reagent (10-acetyl-3,7-dihydroxyphenoxazine; Molecular Probes Europe BV, Leiden, The Netherlands) as described previously.[16] The lysates corresponding to 5−30 μg of total protein were incubated for 30 min at 37 °C in 200 μL of Krebs Ringer phosphate glucose (KRPG) buffer [145 mM NaCl, 5.7 mM sodium phosphate, 4.86 mM KCl, 0.54 mM $CaCl_2$, 1.22 mM $MgCl_2$, and 5.5 mM glucose (pH 7.35) with 1 mM clorgyline]. Semicarbazide (1 mM) was added to the parallel wells to determine the specific hAOC3 activities. After the incubation, Amplex Red, horseradish peroxidase, and substrate (1−1000 or 1−10000 μM) were added. Fresh hydrogen peroxide (250−917 nM) in KRPG was used as a standard. The reaction mixtures were incubated at 37 °C for 10−60 min. The fluorescence values of the duplicate samples were measured with a fluoropolarometer (TECAN Ultra, Tecan, Zürich, Switzerland) with excitation at 545 nm and emission at 590 nm. The specific hAOC3 activity in the transfected lysate was calculated as the proportion of hydrogen peroxide formation inhibited by semicarbazide after subtraction of the corresponding value for the plain HEK 293 EBNA cells. The averages of duplicate wells were used for the calculation. Tyramine quenches the resofurin fluorescence in the Amplex Red assays (up to 90% by 10 mM tyramine). To correct for the quenching, we generated a series of hydrogen peroxide standard curves with 0−10000 μM tyramine. To compensate for the loss of observed fluorescence in the measured samples, we then normalized the results to 0 μM tyramine.

For kinetic analysis, the activities corresponding to 1 μg of total protein and 100% of hAOC3 positive cells were plotted as a function of substrate concentration. The data were fitted to the Michaelis−Menten equation with or without substrate inhibition by nonlinear regression (GraphPad, GraphPad Software Inc.).

Ligand Docking. The crystal structure of sAOC3 in the off-copper conformation was used in the ligand docking studies. The active TPQ conformation was modified to an iminoquinone; the residues were mutated *in silico* with SYBYL 8.0 (Tripos Inc., St. Louis, MO), and the side chain orientations of Met211Val and Tyr394Asn were rotated to optimal positions. Hydrogens were added to the hAOC3 structures with SYBYL 8.0. The ligands were built with SYBYL 8.0 and docked with GOLD Suite 4.0.[47,48] The ligands were covalently connected to the N5 atom of the iminoquinone to simulate the substrate Schiff base intermediate in the enzymatic reaction pathway. The side chains of residues Tyr384, Phe389, Leu468, and Leu469 were allowed to rotate according to the internal rotamer libraries in GOLD Suite 4.0. Ten dockings with each ligand were visually inspected. The cavities in the sAOC3 X-ray structure and structural models of the mutants were calculated with SURFNET.[49] All the structural figures were made with PyMOL.[50] The multiple-sequence alignment was constructed using MALIGN[51] in the Bodil visualization and modeling package.[52]

RESULTS

Crystal Structure of sAOC3. Here we report two crystal structures of human sAOC3, which were refined to 2.6 and 2.95 Å with final R_{cryst} values of 17.5% (R_{free} = 21.3%) and 17.9% (R_{free} = 21.4%), respectively (Table 1). The electron density quality was good throughout both structures (see Figure S3 of the Supporting Information). Both structures contain a homodimer in the asymmetric unit comprising monomers A and B, which are related by 2-fold noncrystallographic axes. The 2.6 Å structure comprises residues A55−A202, A206−A761, B57−B743, and B749−761, whereas the 2.95 Å structure contains residues A58−A202, A206−A742, A749−A761, B56−B202, B206−B743, and B748−B761. The final models do not include residues at the N-terminus (26−55/58). As in the other CAO structures, each monomer is composed of three domains (D2, D3, and D4). Tyr471 is post-translationally modified and modeled as TPQ. One copper ion, two calcium ions, and four N-glycans at residues 137 (N1), 232 (N2), 592 (N4), and 666 (N6) were modeled in each monomer in both structures. Both structures (2.6 and 2.95 Å) are almost identical, apart from some differences in the active site (discussed below). Their structural superimposition gives a root-mean-square deviation (rmsd) of 0.21 Å for 1200 C_α atoms.

Active Site Structure. The active site is buried deep in the D4 domain of each subunit. At the active site, Cu(II) is coordinated by five ligands, which include three histidines (His520, His522, and His684), a water molecule, and either another water

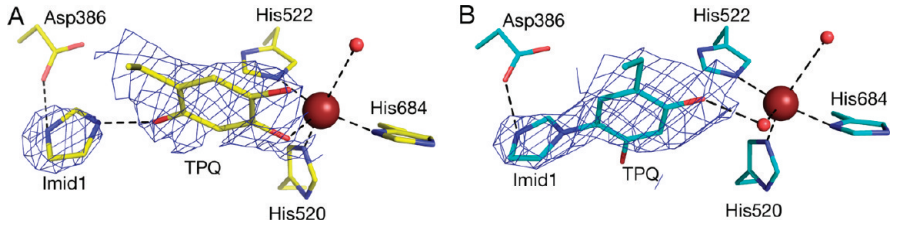

Figure 1. TPQ conformations of the sAOC3 structures in the active site. (A) In the on-copper structure, imidazole is hydrogen bonded to TPQ. The omit map contoured at 1.0σ (blue mesh) is shown for TPQ and imidazole (Imid1). (B) In the off-copper structure, imidazole is covalently bonded to TPQ. Residues are shown as sticks: yellow (on-copper) or cyan (off-copper) for carbon, blue for nitrogen, red for oxygen and water, and brown for Cu(II).

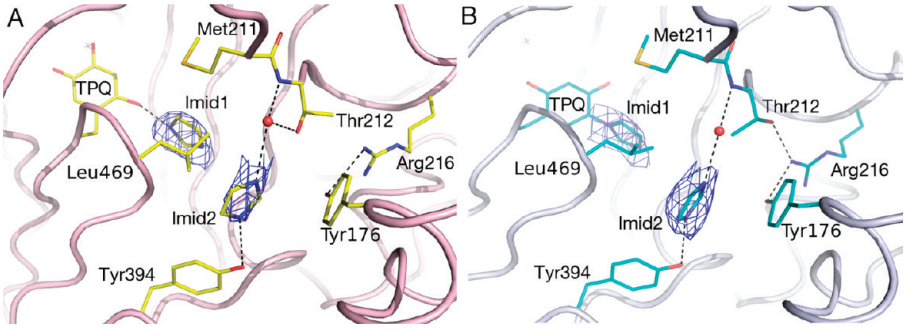

Figure 2. Substrate channel showing the second binding site for imidazole. (A) Monomer B of the on-copper structure (light pink cartoon). Thr212 is hydrogen bonded to the water molecule, which mediates its interaction with imidazole (Imid2). (B) Monomer B of the off-copper structure (gray cartoon). Thr212, hydrogen bonded with Arg216, keeps the same conformation in monomer A of both on-copper and off-copper structures. Residues discussed in the text are shown as sticks: cyan (off-copper) or yellow (on-copper) for carbon, blue for nitrogen, red for oxygen, and orange for sulfur. The omit map contoured at 1.0σ (blue mesh) is shown for the imidazole molecules.

molecule or TPQ (Figure 1). In each subunit of the 2.6 Å structure, an oxygen atom at position 4 (O4) of TPQ binds to Cu(II) at the fourth position in an on-copper inactive state and a water molecule coordinates the fifth position (Figure 1A), whereas in our 2.95 Å structure, two water molecules occupy the fourth and fifth positions and TPQ points away from the Cu(II) ion and is in the off-copper active state (Figure 1B). Hereafter, the on-copper and off-copper structures refer to the 2.6 and 2.95 Å structures, respectively. In both the on-copper and off-copper structures, the oxygen atom of the water at the fifth position is 2.9−3.1 Å from the Cu(II) ion, compared to the distances of 1.9−2.2 Å from its other ligands. This Cu(II) coordination can be described as a distorted square pyramidal, which is similar to the Cu(II) coordination seen in an active form of the *E. coli* CAO structure.[53]

Imidazole Binding Sites. In the active site, TPQ makes contacts with an imidazole molecule (Imid1) in each subunit of both crystal structures (Figure 1). In the on-copper structure, O2 of TPQ is hydrogen bonded to N1 of Imid1, while in the off-copper structure, C5 of TPQ is covalently bonded to imidazole (Figure 1). The position of the imidazole molecule is the same in both structures. In addition, N3 of Imid1 (opposite of TPQ) forms a hydrogen bond with Asp386 in both structures (Figure 1). Furthermore, another imidazole molecule (Imid2) is modeled in the substrate channel where it forms a hydrogen bond to Tyr394 and makes a water-mediated contact with the main chain nitrogen of Thr212 (Figure 2). The OH group of Thr212 interacts directly with the same water molecule only in monomer B of the on-copper structure (Figure 2A), whereas in both chains of the off-copper structure and chain A of the on-copper structure, Thr212 is in a different conformation and participates in the hydrogen bonding network of Arg216 and Tyr176 (Figure 2B). In addition, Imid2 forms hydrophobic contacts with Leu469 and Tyr176. Away from the active site, two more imidazole molecules (Imid3 and Imid4) are hydrogen bonded to Thr477 in each monomer of both structures (Figure S4 of the Supporting Information). They are located in a hydrophobic pocket formed by Pro347, Ile349, Leu365, Val462, Trp475, Ile487, and Phe526. Imid4 forms an additional hydrogen bond to Ser464.

Calcium Sites. As in the other AOC3 structures, two calcium ions are present on the molecular surface of each subunit in both structures. In the on-copper structure, one calcium ion is coordinated to six oxygen atoms from residues Asn665, Glu572, and Glu667, the main chain carbonyl of Phe663, and two water molecules in an octahedral geometry. The second calcium ion coordinates Asp529, Asp531, Asp673, the main chain carbonyl of Leu530 and Leu674, and a water molecule. The coordination of the calcium ions is similar in the off-copper structure, except that the two water molecules were not resolved at the first calcium site.

Disulfide Bridges. Our previous hAOC3 structures showed an intermonomer disulfide bridge between Cys748 residues,[27] whereas others have modeled an intramonomer disulfide bridge between Cys748 and Cys41.[28,30] In both of the sAOC3 structures, the electron density for Cys748 can be traced in only one of the monomers: chain A of the on-copper structure and chain B of the off-copper structure. Also, Cys41 is disordered. Thus, Cys748 does not form any disulfide bridge. All other disulfide bridges in sAOC3 are consistent with the other previously determined hAOC3 structures.

Effect of Imidazole on TPQ Reactivity. The UV−visible absorption spectra of the TPQ cofactor of sAOC3 in the presence

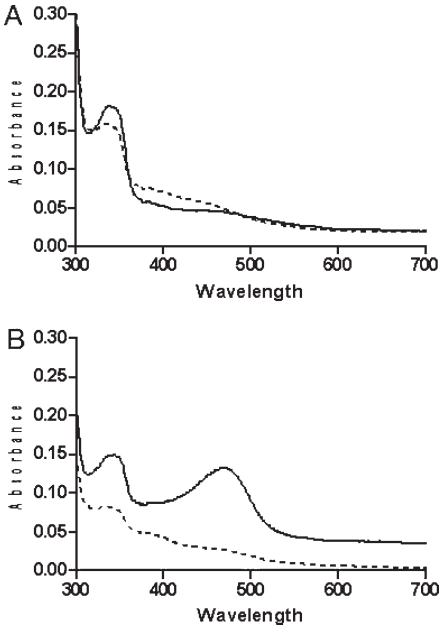

Figure 3. UV−visible absorption spectra of sAOC3. (A) Native sAOC3 with (---) or without (—) imidazole. (B) After treatment with *p*-NPH.

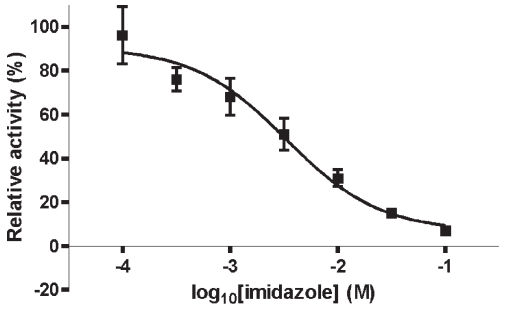

Figure 4. Imidazole and hAOC3 activity. The effect of imidazole (10^{-4}−10^{-1} M) on the hAOC3 amine oxidase activity was assayed by monitoring the formation of ^{14}C-labeled benzaldehyde. The relative activities (mean ± standard deviation) with respect to reaction without imidazole are presented. The background activity with 1 mM semicarbazide is subtracted from each value. The reactions were performed in triplicate.

or absence of imidazole were used to study its effect on the *p*-NPH derivatization of the TPQ cofactor (Figure 3). *p*-NPH forms a covalent complex with the TPQ cofactor with a characteristic visible absorbance peak at 457−463 nm at neutral pH.[54] After treatment with *p*-NPH, the spectrum of sAOC3 without imidazole has a clear peak at 469 nm, which corresponds to a hydrazone adduct of the protein. In the presence of imidazole, the sAOC3 spectra did not show that peak, suggesting that imidazole prevents derivatization of TPQ by *p*-NPH (Figure 3B).

Effect of Imidazole on hAOC3 Activity. The effect of imidazole on recombinant hAOC3 enzymatic activity was assayed by monitoring the formation of radioactive benzaldehyde from ^{14}C-labeled benzylamine (Figure 4). Imidazole clearly inhibited hAOC3 activity, and the inhibition is fitted to a one-site competition model (IC_{50} of 1.28−8.6 mM with 95% confidence intervals, 20 min preincubation). At the imidazole concentration of 100 mM used in the sAOC3 crystallization, 93% of the activity was inhibited. The activity of CHO mock lysate remained at the background level, and it was not affected by the different imidazole concentrations (results not shown).

Mutations. We have previously generated a triple mutant (Met211Val/Tyr394Asn/Leu469Gly)[10] that changed the substrate binding preferences of hAOC3 to resemble those of hAOC2. In this study, we mutated these residues in hAOC3 individually to the corresponding ones in hAOC2, (i.e., Met211Val, Tyr394Asn, and Leu469Gly) to investigate their individual roles in human hAOC3 activity. In addition, Thr212, which was assumed to be O-glycosylated,[55] was mutated to alanine to determine if it has any effect on hAOC3 function. All mutations were confirmed by sequencing. The mutations did not affect the recognition of the transfected cells by the anti-hAOC3 antibody, and therefore, the transfection efficiency was confirmed by FACS counting. The expression levels of the mutants on the cell surface were comparable to that of the wild type (WT) (data not shown).

Enzymatic Activity of the Mutants. Although both hAOC2 and hAOC3 are monoamine oxidases, they prefer different substrates: hAOC2 oxidizes large substrates better than hAOC3.[10] To study the individual effect of four mutants, Met211Val, Thr212Ala, Tyr394Asn, and Leu469Gly, on hAOC3 activity, we measured H_2O_2 production by the WT hAOC3 and mutant cell lysates. We also measured the activities of a previously reported triple mutant, Met211Val/Tyr394Asn/Leu496Gly, for comparison. We used four different substrates: benzylamine (BZ), methylamine (MA), 2-phenylethylamine (PEA), and *p*-tyramine (TYR). The kinetic curves for BZ and MA oxidation by WT and the mutants were fitted to the Michaelis−Menten equation, because no evident substrate inhibition was detected (Figure 5). The derived kinetic parameters for BZ and MA oxidation are listed in Table 2

BZ is a commonly used substrate for hAOC3. The Michaelis−Menten constants, K_M(BZ), for Met211Val and Leu469Gly markedly decreased to 14 and 7% of the WT value, respectively. K_M for the triple mutant decreased to 10% of the WT value. Thr212Ala had a significant but smaller effect, as K_M(BZ) was lowered to 45% of the WT value. Tyr394Asn, on the other hand, experienced a 17% increase in the K_M(BZ) value. V_{max} values of the mutants remained close to that of WT, except for Leu469Gly, whose V_{max}(BZ) was double compared to that of WT, and the triple mutant, whose V_{max}(BZ) was lowered to ∼30% of the maximal reaction rate of WT.

When MA oxidation was assayed, the Thr212Ala mutation increased K_M(MA) approximately 2-fold, Tyr394Asn ∼4-fold, and the triple mutant ∼6-fold. Other mutations somewhat decreased K_M(MA): the Leu469Gly value was ∼70% and the Met211Val value ∼84% of the WT K_M(MA). The largest changes were seen for V_{max}, which was reduced ∼10-fold for Leu469Gly and 23-fold for Met211Val and also decreased to ∼50% for Thr212Ala and Tyr394Asn and 33% for the triple mutant.

Even though PEA is a known substrate for hAOC3, we were not able to measure kinetic values with accuracy, because of the low activity of hAOC3 toward PEA. Therefore, we compared the activities at a single concentration, 500 μM PEA (Figure 5C). This concentration was used, because it was the lowest concentration at which we could detect any activity for WT, so that the comparison to WT was possible. For Met211Val and Tyr394Asn, we could detect only some, nearly background activity at 500 μM PEA. Thr212Ala activity was nearly at the WT level (74% of WT activity), but the activities of both

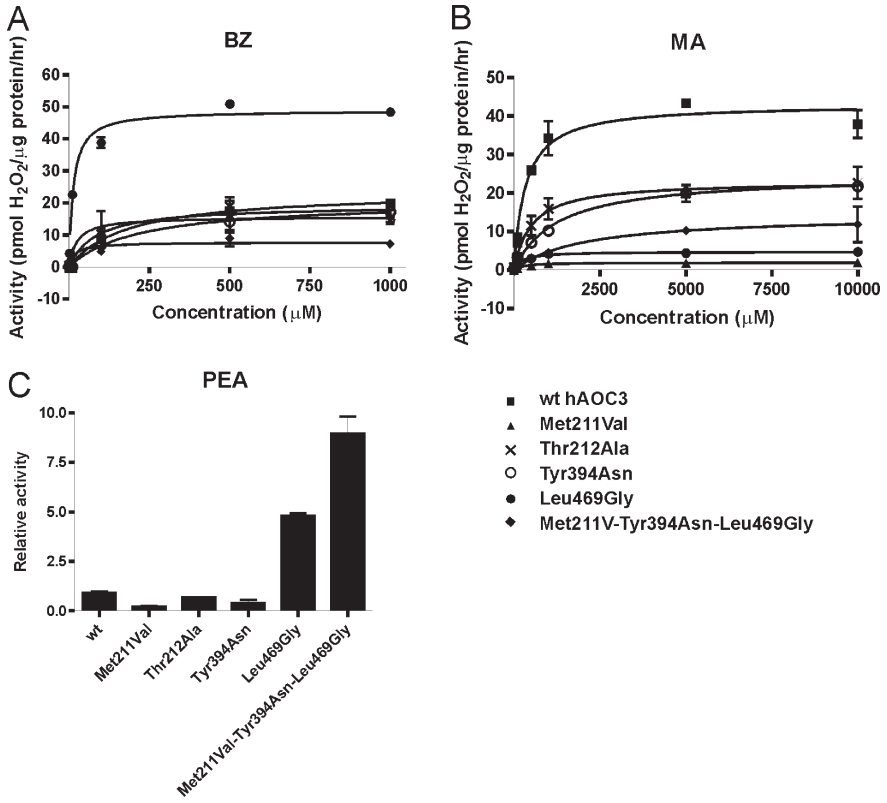

Figure 5. Amine oxidase activity assays (mean ± standard deviation). Kinetic curves of WT hAOC3 and mutant proteins for BZ (A) and MA (B) oxidation. The activities relative to WT at 500 μM PEA are presented in panel C.

Table 2. Kinetic Parameters Determined for WT and Mutant hAOC3s

	K_M (μM)	V_{max} (pmol μg^{-1} h^{-1})	V_{max}/K_M
	Benzylamine (BZ)		
WT	184 ± 31	24 ± 1.1	0.13
Met211Val	25 ± 21	16 ± 2.3	0.64
Tyr394Asn	215 ± 49	21 ± 1.4	0.10
Leu469Gly	13 ± 2.4	49 ± 2.4	3.8
Thr212Ala	84 ± 33	19 ± 1.7	0.22
Met211Val/Tyr394Asn/Leu469Gly	18 ± 14	7.7 ± 0.95	0.43
	Methylamine (MA)		
WT	331 ± 77	43 ± 2.1	0.06
Met211Val	280 ± 36	1.9 ± 0.05	0.007
Tyr394Asn	1260 ± 157	25 ± 0.09	0.02
Leu469Gly	236 ± 36	4.8 ± 0.2	0.02
Thr212Ala	502 ± 161	23 ± 1.8	0.05
Met211Val/Tyr394Asn/Leu469Gly	2043 ± 1146	14 ± 2.6	0.007

Leu469Gly and the triple mutant were markedly increased (~5- and ~10-fold, respectively). For Leu469Gly, we determined the K_M(PEA) to 1852 ± 1037 μM and the V_{max} to be 25 ± 10 pmol of H_2O_2 h^{-1} (μg of protein)$^{-1}$ using the Michaelis–Menten equation with substrate inhibition. In addition, we observed substrate inhibition characteristic of hAOC3 (K_i = 2.7 mM). The K_M(PEA) for Leu469Gly is 4 times greater than the K_M(PEA) for the triple mutant (478 μM[10]), but the V_{max} is similar [18 pmol of H_2O_2 h^{-1} (μg of protein)$^{-1}$ for the triple mutant[10]].

The kinetic constants could not be determined for any of the measured proteins with 0–10 mM TYR. At the highest TYR concentration, Leu469Gly had the highest activity [243 pmol of H_2O_2 h^{-1} (μg of protein)$^{-1}$] and Met211Val was also active [118 pmol of H_2O_2 h^{-1} (μg of protein)$^{-1}$], while the activities of the other mutants and WT remained at the background level [<10 pmol of H_2O_2 h^{-1} (μg of protein)$^{-1}$].

Substrate Docking Studies. To assess the mechanism of binding of the substrate to hAOC3, we performed docking studies with BZ, PEA, and TYR on the Met211Val and

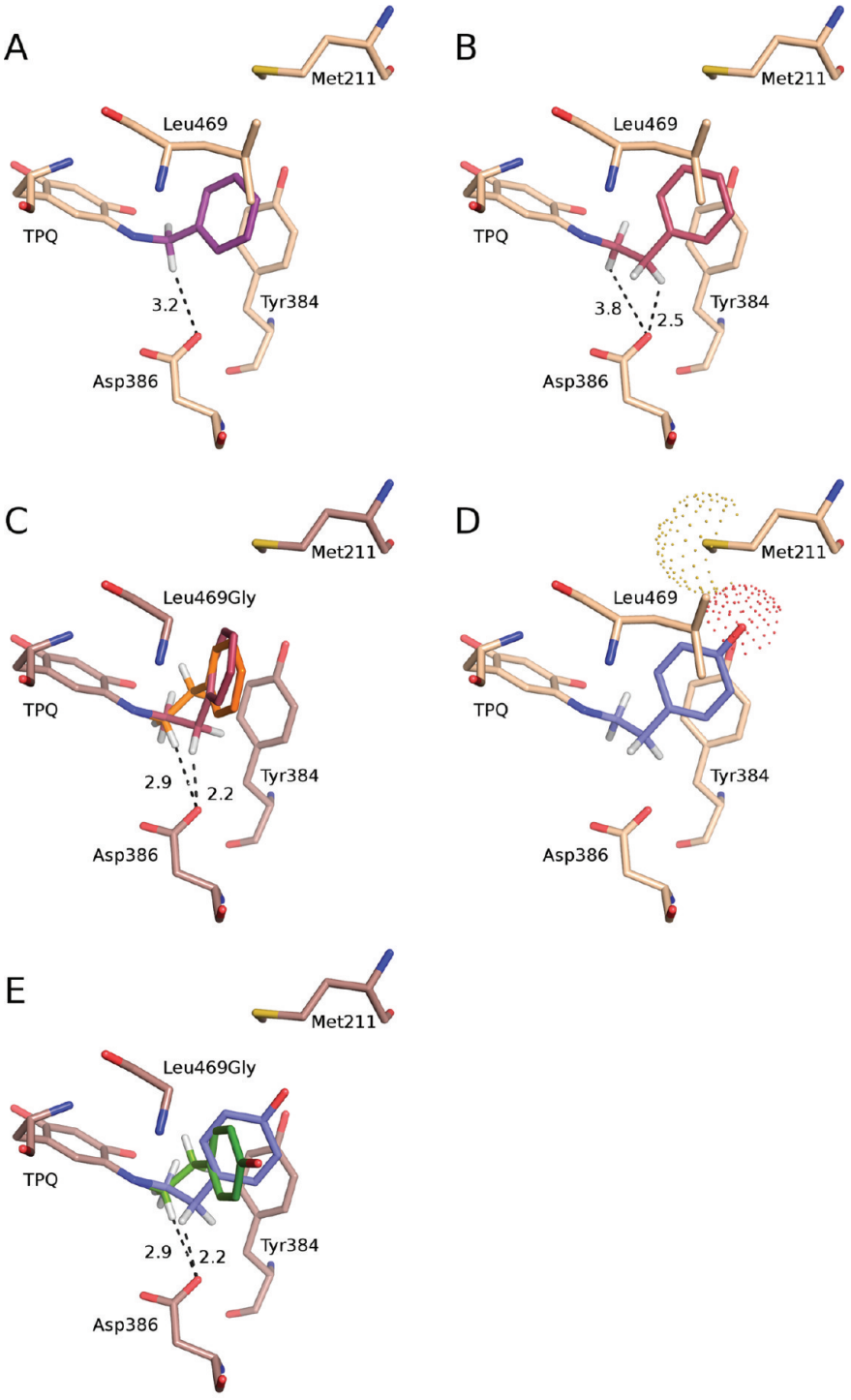

Figure 6. Representative docking results for (A) WT hAOC3 and BZ, (B) WT hAOC3 and PEA, (C) the Leu469Gly mutant and PEA, (D) WT hAOC3 and TYR, and (E) the Leu469Gly mutant and TYR. The amino acids are labeled, and distances are given in angstroms. See the text for details.

Leu469Gly mutants and WT. MA was not docked because of its small size. Dockings were performed for the Tyr394Asn mutant but are not presented here because the residue is too far from the TPQ to influence the docking of the tested substrates, and thus, the docking results were comparable to the WT results. For the same reason, the Thr212Ala mutant was excluded from the docking experiments. In the calculations, the substrates were covalently linked to TPQ to mimic the substrate Schiff base intermediate (Scheme 1). The side chains of Tyr384, Phe389, Leu468, and Leu469 were allowed to adopt different conformations in the docking process, thus introducing some flexibility into the active site. In all docking results, the side chain of Leu469 adopts a different conformation than in the crystal structure and, thus, enlarges the active site. The aromatic ring of the docked BZ is packed between Tyr384 and Leu469 in WT hAOC3, with the (*R*) C_α hydrogen of BZ positioned 3.2 Å from the catalytic base

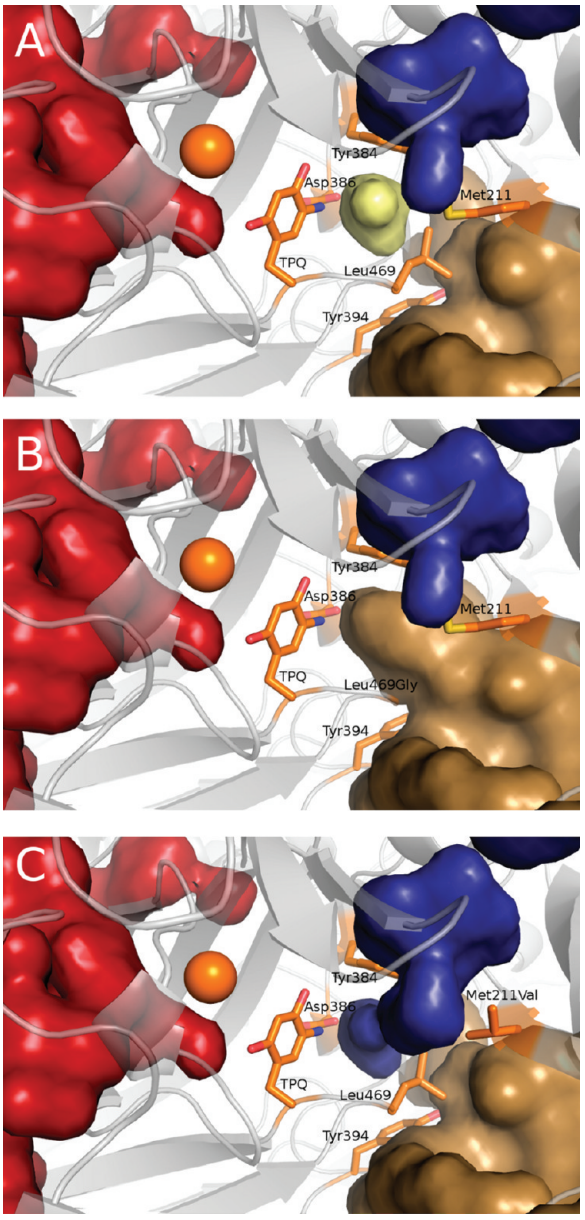

Figure 7. Cavities in (A) WT hAOC3, (B) the Leu469Gly mutant of hAOC3, and (C) the Met211Val mutant of hAOC3. The interfacial cavity is colored red, the active site cavity pale yellow, the active site channel brown, and the water channel blue.

Asp386 (Figure 6A). In all the mutants, BZ is docked in the approximately same orientation as in WT hAOC3, stacking with Tyr384 (Figure 6A).

In WT hAOC3, PEA is docked in several poses, but in all of them, the aromatic ring of PEA stacks with Tyr384 and forms hydrophobic interactions with Leu469 (Figure 6B). The C_β hydrogens of PEA are closer to Asp386 than the C_α hydrogens in the best-ranked poses (Figure 6B). As in WT, PEA is docked in several poses in the Leu469Gly mutant (Figure 6C), but in all the poses, the aromatic ring of PEA is positioned farther from Tyr384 than in WT hAOC3, which is possible because of the additional space provided by the replacement of Leu469 by the much smaller glycine residue. In some poses, the C_β hydrogens of PEA are closest to Asp386 (Figure 6C; carbon atoms of PEA colored ruby), while in others, it is the C_α hydrogen (Figure 6C; carbon atoms of PEA colored orange). Both conformations have similar fitness values.

TYR is docked in poses similar to those of PEA, but in WT hAOC3, the hydroxyl group of TYR and the large sulfur atom of Met211 are in the proximity of each other (Figure 6D). In the Leu469Gly mutant, TYR is partially docked in poses similar to those of PEA (Figure 6E; carbon atoms of TYR colored blue). However, in some poses, the aromatic ring of TYR is twisted compared to PEA and the C_α hydrogens are close (3 Å) to the catalytic Asp386 (Figure 6E; carbon atoms of TYR colored green). According to the docking results, there is no apparent hydrogen bonding partner for the hydroxyl group of TYR in hAOC3, but TYR might form water-mediated hydrogen bonds to the active site residues.

Cavities. To visualize the effect of the Met211Val, Thr212Ala, Tyr394Asn, and Leu469Gly mutations on the hAOC3 cavities, the surfaces of the substrate channel, the active site cavity, the interface (central) cavity, or lake, and a water channel were calculated for hAOC3 and the mutants. The water channel has been suggested to act as a proton relay system that accelerates the completion of the reaction cycle.[56] It extends toward the surface, but the side chains of four amino acids (His242, Glu246, Ser376, and Ala498) block the route to the surface. In the mutant enzymes, the Leu469Gly and Met211Val mutations have the largest effects on the shapes and sizes of the cavities. In WT hAOC3, the substrate channel is separated from the active site cavity by the side chain of Leu469 (Figure 7A), while these cavities are linked in the Leu469Gly mutant (Figure 7B). In contrast, in the Met211Val mutant, the active site cavity is connected to the water channel but not to the substrate channel (Figure 7C).

DISCUSSION

Overall X-ray Structure of sAOC3. We report here two X-ray structures of a natural form of AOC3, namely, sAOC3 extracted from human plasma. These sAOC3 crystals were obtained from the same conditions as our previous hAOC3 structures.[27] The sAOC3 structures are in general very similar to the published hAOC3 structures[27,28,30] despite the lack of one of the disulfide bridges, which in the previously known hAOC3 structures is either intermonomeric[27] or intramonomeric[28,30] and formed between two Cys748 residues or between Cys748 and Cys41, respectively. In the sAOC3 structures determined in this study, Cys748 seems to be in a reduced form. This is similar to the case in previous studies in which the corresponding cysteine may connect the hAOC1 dimer with an intermonomeric disulfide bond or may be in a reduced state.[29,57] Therefore, we suggest that this C-terminal cysteine can exist in reduced or oxidized states, which either might be a consequence of radiation damage as suggested previously[57] or might be driven by hydrogen peroxide, one of the products of the sAOC3-catalyzed reaction.

The TPQ-Bound Imidazole Has Different Binding Modes. Although the two sAOC3 structures are crystallized under similar conditions, the TPQ cofactors are in different conformations: active off-copper and inactive on-copper. The flexibility of TPQ has been shown in previous studies, where TPQ was in the on-copper and off-copper conformations even within the same crystal.[58] Furthermore, an imidazole derived from the crystallization buffer is bound to TPQ in both sAOC3 structures. In the on-copper structure, Imid1 forms a hydrogen bond with TPQ, whereas in

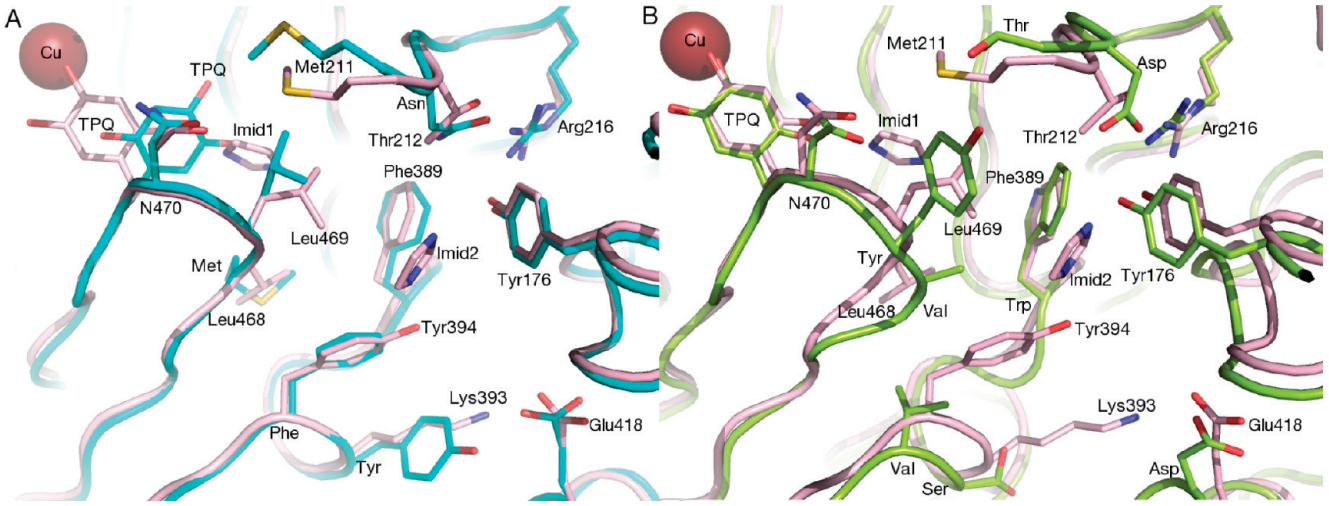

Figure 8. sAOC3 on-copper structure superimposed on BSAO and hAOC1. (A) sAOC3 and BSAO (PDB entry 1TU5). (B) sAOC3 and hAOC1 (PDB entry 3HI7). The cartoon loop structure of the on-copper sAOC3 structure is colored light pink, and BSAO and hAOC1 are colored cyan and light green, respectively. Residues in the substrate channel and active site are shown as sticks. Only sAOC3 residues are numbered. The structures were aligned with PyMOL.[50]

the off-copper structure, it binds covalently to TPQ. In the previous studies, the imidazole in the active site of the *Pichia pastoris* CAO (PDB entries 1RKY[58] and 1W7C[59]) and the imidazoline ring of clonidine in the BSAO structure (PDB entry 2PNC[26]) interact similarly with the on-copper conformation of TPQ (Figure S5 of the Supporting Information). Thus, we report for the first time an imidazole adduct of TPQ formed by a covalent bond between imidazole and the off-copper conformation of TPQ.

To clarify the role of imidazole at the hAOC3 active site, we measured the effect of imidazole on the hAOC3 activity. At 100 mM imidazole, the hAOC3 activity was significantly reduced (Figure 4). Furthermore, we confirmed that imidazole prevents the derivatization of TPQ by *p*-NPH either by binding directly to TPQ or by blocking access to TPQ (Figure 3). The shallowness of the Hill slope (Figure 4) suggests that imidazole inhibits hAOC3 in a rapidly reversible manner, and we were able to demonstrate almost uninhibited activity of hAOC3-expressing CHO cells after removal of imidazole (data not shown). The inhibitory effect of a high imidazole concentration has actually been reported long ago for pig plasma amine oxidase.[60] More recently, efficient inhibition and covalent binding of secondary amines to TPQ have been reported in BSAO.[61] The re-examination of our earlier published hAOC3 structures[27] revealed unexplained electron density close to TPQ, which now could be interpreted as an imidazole in the active site. As the active site is very conserved in CAOs, we suggest that other CAOs might equally bind imidazole, and thus, it might disturb crystallization of CAO−inhibitor complexes.

The Second Binding Site for Imidazole Is Located near Thr212. Surprisingly, our sAOC3 structures show an additional binding site for imidazole in the vicinity of Thr212 and Tyr394 in the substrate channel. Thr212 was earlier suggested to be O-glycosylated, based on theoretical prediction and undefined electron density in the previously determined hAOC3 structures.[27] However, a sugar unit does not fit into the improved electron density maps of the sAOC3 structures, and mass spectrometry analysis showed that Thr212 was not glycosylated (data not shown). Instead, imidazole can easily be fitted into the density, thus revealing a secondary binding site for imidazole in sAOC3 (Figure 8). The Imid2 molecule in this newly identified position is hydrogen bonded directly to Tyr394 and via a water molecule to the Thr212 backbone. Moreover, in one of the four sAOC3 subunit structures, Imid2 forms a hydrogen bond with the side chain hydroxyl of Thr212. In the other sAOC3 subunits, the side chain of Thr212 interacts with Arg216, which is further hydrogen bonded to Tyr176. In addition to the residues mentioned above, Phe389 is in contact with Imid2. Because the Tyr394Asn and Thr212Ala mutations had only small effects on the hAOC3 activity and Imid2 primarily makes contact with the side chain of Tyr394 and the main chain of Thr212, we speculate that the effect of these mutations on substrate specificity was not due to disturbance of the secondary binding site but rather a result from the enlargement of the substrate channel by Tyr394Asn or the enlargement of the entrance to the active site by Thr212Ala. This would explain the difference in their activity toward BZ and MA compared to that of WT. This is in line with the recent study with two different *Hansenula polymorpha* amine oxidases (HPAOs), which have different substrate specificities: HPAO-2 with a wider entrance to the active site better oxidizes bulkier BZ than smaller MA, whereas HPAO-1 with a narrower entrance is more efficient toward MA than BZ.[62] Thus, Thr212 seems to function as an additional gate residue together with Leu469 and Tyr384. The corresponding residue in the hAOC1 structure, Asp186, which interacts with the triazene group of the berenil inhibitor, has been suggested to be important for the diamine specificity because it is conserved in all diamine oxidases.[57] This further pinpoints the importance of the residue in this position for the CAO activity.

Actually, a secondary imidazoline binding site has been previously suggested for CAOs.[60,63] However, on the basis of our structural and enzymatic activity data, the imidazole binding site in the substrate channel of the sAOC3 structure differs from the allosteric imidazoline binding site presented for BSAO.[26] In fact, this site seems to be unique for human AOC3. The residues corresponding to Thr212 and Tyr394 in AOC3 are Asn211 and Phe393 in BSAO, respectively (Figure 8 and Figure S6 of the Supporting Information). Unlike Tyr394 in AOC3, Phe394 in

BSAO cannot form a hydrogen bond with Imid2, and thus, it is likely that BSAO lacks the second imidazole-binding site. This site is conserved neither in hAOC1 nor in hAOC2 (the corresponding residues are Asp186 and Val381 in AOC1 and His206 and Asn388 in AOC2). However, the hydrogen bonding network of arginine and tyrosine (Arg216−Tyr176 in AOC3) is conserved in BSAO and hAOC1 and involves the residue corresponding to Thr212 in AOC3 (Asn211 in BSAO and Asp186 in AOC1[8]). The arginine−tyrosine hydrogen bond is actually conserved in mammalian AOC1 and AOC3 sequences, indicating its important role in shaping the substrate channel (Figure S6 of the Supporting Information). Furthermore, the comparison of the Imid2 binding site reveals that the residue corresponding to Phe389 is a tryptophan in AOC1 whereas it is conserved in BSAO and AOC2 (Figure 8).

Leu469 and Met211 Are Important for Substrate Specificity. Because a triple mutant (Met211Val/Tyr394Asn/Leu469Gly) is known to change the substrate specificity of hAOC3,[10] we generated single-point mutants to study the individual roles of Met211, Tyr394, and Leu469. We explored the effect of these point mutations on the enzymatic activity of hAOC3 and analyzed the data in light of computational docking studies and the sAOC3 structures. This assumes that the rate-determining step in WT hAOC3, as in BSAO, is in the reductive half-reaction.[64,65] If this is not the case, then the effect of the mutations is likely underestimated, as presumably they are mainly manifested in the reductive half-reaction. On the basis of this assumption, our results pinpoint that two of the residues, Leu469 and Met211, are important for the hAOC3 substrate recognition. Mutation of either of these residues to the corresponding one in hAOC2 (glycine and valine, respectively) changes the substrate preference profile of the hAOC3 enzyme. The observed differences in the enzymatic activity were studied by docking BZ, PEA, and TYR to the crystal structure of off-copper sAOC3 and to the modeled structures of the mutants. The fourth tested substrate, MA, was not docked because of its small size. However, the apparent decrease in the maximal reaction rate of MA in all of the mutations shows that the enlargement of the active site is not beneficial for MA oxidation by hAOC3. It seems that the larger active site of the Met211Val and Leu469Gly mutants and the absence of large hydrophobic side chains make the correct positioning of small MA difficult. Moreover, the critical effect of the size of the active site is stressed in the case of the triple mutant (Mel211Val/Tyr394Asn/Leu469Gly) because it also has a 3-fold lower maximal reaction rate than WT for MA oxidation and the K_M is 6 times higher than for WT.[10]

The mutation of gate residue Leu469 to glycine had the largest effect on the enzymatic properties of hAOC3. The Leu469Gly mutation increased the level of hAOC3 oxidation of BZ more than 10-fold and the level of oxidation of PEA almost 10-fold. In addition, the mutant protein was able to oxidize TYR in contrast to WT. The docking studies gave a possible explanation for the acquired ability of Leu469Gly to oxidize PEA and TYR: the substrates were docked in poses that positioned their C_α hydrogens 3 Å from the catalytic Asp386, allowing the abstraction of these hydrogens and the progression of the oxidation reaction (Figure 6C,E). In the Leu469Gly model, the active site is open and substrates can reach and bind to TPQ more easily (Figure 7B). BZ was docked in the Leu469Gly mutant in the same pose as in WT hAOC3, and thus, the increased activity and reaction rate of the mutant are likely to result from the absence of the proposed active site gate Leu469.[27,28,66] The gating function of Leu469 is further supported by the fact that Met211Val and Tyr394Asn mutations failed to improve the PEA oxidation, but triple mutant Met211Val/Tyr394Asn/Leu469Gly[10] has gained this function. These results also pinpoint the fact that the mutations are not additive.

The Met211Val mutant increased BZ activity (K_M) compared to that of WT. The explanation for the increased BZ activity of the mutant compared to that of WT might lie in the changes of the cavity architecture, because the docking experiments did not reveal any differences in the proposed binding mode. In the Met211Val mutant, the change of methionine to a smaller and less flexible valine exposes the active site cavity to a water channel, whereas in the WT enzyme, these cavities are separate (Figure 7C). Nurminen et al. have also reported that the flexibility of Met211 during molecular dynamics simulations opens access to the same channel (called the side pocket in their work).[67] The water channel is thought to be involved in the proton transfer system,[56,68] and unhindered access from the active site could accelerate the second half of the reaction. In the case of PEA, the computational docking studies suggest that the poor hAOC3 activity on PEA results from the bad positioning of the C_α hydrogens to be abstracted by the catalytic Asp386. This inhibits the removal of the proton of both Met211Val and WT. Therefore, the opened access to the water channel, which could facilitate the proton transfer, has no effect here. This could, however, explain why the triple mutant is ∼2 times better in oxidizing PEA compared to the Leu469Gly mutant. In the triple mutant, the open access both to the active site (Leu469Gly mutation) and to the water channel (Met211Val mutation) further facilitates the reaction. Albeit the docking calculations similarly suggested a bad positioning of C_α hydrogens for TYR, we observed improved oxidation of TYR compared to that of WT. Even though PEA and TYR are almost of the same size, the additional hydroxyl group in TYR might form water-mediated hydrogen bonds to residues in the substrate channel and, thus, allow the substrate to adopt a pose that is more favorable for the catalytic reaction. In general, the amino acid substitutions might lead to local structural changes in the active site of the mutants, which could allow different positioning of the substrates. On the basis of the BSAO and sAOC3 X-ray structures, both Met211 and Leu469 actually adopt different conformations (Figure 8), and in molecular dynamics simulations, their side chains were flexible.[67] TPQ is flexible in general,[69] which further supports the possibility of local rearrangements in the active site.

In conclusion, the new X-ray structures of native human sAOC3 reveal two imidazole binding sites in the substrate channel: the first site located in the vicinity of TPQ and the second novel site flanked by Thr212 and Tyr394. Moreover, we show that Met211 is a key residue for substrate specificity and/or positioning and demonstrate the gating function of Leu469 by mutational and activity studies. In addition, computational studies suggest that an enlarged gate seen in both the Leu469 and Thr212 mutants greatly affects substrate preferences. These findings open up intriguing possibilities for inhibitor design based on secondary amine inhibition and/or providing specificity by bridging the active site and the secondary imidazole binding site that appears to be unique in hAOC3.

■ ASSOCIATED CONTENT

Supporting Information. Figures S1 and S2 describe electron density maps to support the off-copper state of the 2.95 Å

structure. Figure S3 shows the electron density quality of the on-copper structure. Figure S4 shows the two imidazole binding sites outside the active site in the on-copper structure. Figure S5 illustrates the active site comparison of selected AOC structures. Figure S6 shows a multiple-sequence alignment of mammalian (human, bovine, mouse, and rat) AOC sequences. This material is available free of charge via the Internet at http://pubs.acs.org.

Accession Codes

The structural coordinates have been deposited in the Protein Data Bank as entries 2Y73 and 2Y74.

AUTHOR INFORMATION

Corresponding Author

*E-mail: tiina.salminen@abo.fi. Phone: +358-40 5151201. Fax: +358-2-2305018.

Present Addresses

▽Centre for Drug Research, University of Helsinki, FI-00014 Helsinki, Finland.

●PerkinElmer, FI-20101 Turku, Finland.

Author Contributions

H.E., H.K., and V.P. contributed equally to this work.

Funding Sources

This work was supported by the Sigrid Juselius Foundation (S.J. and T.A.S.), the Tor, Joe and Pentti Borgs Foundation (T.A.S.), Medicinska Understödsföreningen Liv och Hälsa (H.K. and Y.N.), the Academy of Finland [H.E. (132701), Y.N. (121410), and T.A.S. (132998)], Stiftelsens för Åbo Akademi forskningsinstitut (V.P.), and the National Doctoral Programme in Informational and Structural Biology (E.B.).

ACKNOWLEDGMENT

We thank Dr. Jarmo Käpylä and Dr. Gennady Yegutkin for the helpful comments about the enzyme kinetics; Teija Kanasuo, Sari Mäki, Maritta Pohjansalo, Minna Peippo, and Katja Koivula for excellent technical help in the lab; Robin Sundström for assistance with refinement of the structures; and Prof. Mark Johnson for the excellent computing facilities at Åbo Akademi University. Use of Biocenter Finland infrastructure at Åbo Akademi (bioinformatics, structural biology, and translational activities) is acknowledged. We also acknowledge the European Synchrotron Radiation Facility and MAX-lab for provision of synchrotron radiation facilities.

ABBREVIATIONS

hAOC3, human membrane primary amine oxidase; hAOC2, human retina specific amine oxidase; hAOC1, human diamine oxidase; VAP-1, vascular adhesion protein-1; CAO, copper-containing amine oxidase; SSAO, semicarbazide-sensitive amine oxidase; TPQ, topaquinone; BSAO, bovine serum amine oxidase; BZ, benzylamine; MA, methylamine; PEA, 2-phenylethylamine; TYR, *p*-tyramine; sAOC3, human soluble primary amine oxidase; KRPG, Krebs Ringer phosphate glucose; *p*-NPH, *p*-nitrophenylhydrazine; CHO, Chinese hamster ovary; HPAO, *H. polymorpha* amine oxidase; Imid1, imidazole 1; Imid2, imidazole 2.

REFERENCES

(1) Salmi, M., and Jalkanen, S. (1992) A 90-kilodalton endothelial cell molecule mediating lymphocyte binding in humans. *Science 257*, 1407–1409.

(2) Klinman, J. P. (1996) Mechanisms whereby mononuclear copper proteins functionalize organic substrates. *Chem. Rev. 96*, 2541–2562.

(3) Jalkanen, S., and Salmi, M. (2001) Cell surface monoamine oxidases: Enzymes in search of a function. *EMBO J. 20*, 3893–3901.

(4) Lyles, G. A. (1995) Substrate-specificity of mammalian tissue-bound semicarbazide-sensitive amine oxidase. *Prog. Brain Res. 106*, 293–303.

(5) Toninello, A., Pietrangeli, P., Marchi, U. D., Salvi, M., and Mondov, B. (2006) Amine oxidases in apoptosis and cancer. *Biochim. Biophys. Acta 1765*, 1–13.

(6) Dawkes, H. C., and Phillips, S. E. (2001) Copper amine oxidase: Cunning cofactor and controversial copper. *Curr. Opin. Struct. Biol. 11*, 666–673.

(7) Elmore, B. O., Bollinger, J. A., and Dooley, D. M. (2002) Human kidney diamine oxidase: Heterologous expression, purification, and characterization. *J. Biol. Inorg. Chem. 7*, 565–579.

(8) Maintz, L., and Novak, N. (2007) Histamine and histamine intolerance. *Am. J. Clin. Nutr. 85*, 1185–1196.

(9) Imamura, Y., Kubota, R., Wang, Y., Asakawa, S., Kudoh, J., Mashima, Y., Oguchi, Y., and Shimizu, N. (1997) Human retina-specific amine oxidase (RAO): cDNA cloning, tissue expression, and chromosomal mapping. *Genomics 40*, 277–283.

(10) Kaitaniemi, S., Elovaara, H., Grön, K., Kidron, H., Liukkonen, J., Salminen, T., Salmi, M., Jalkanen, S., and Elima, K. (2009) The unique substrate specificity of human AOC2, a semicarbazide-sensitive amine oxidase. *Cell. Mol. Life Sci. 66*, 2743–2757.

(11) Salmi, M., Kalimo, K., and Jalkanen, S. (1993) Induction and function of vascular adhesion protein-1 at sites of infiammation. *J. Exp. Med. 178*, 2255–2260.

(12) Zorzano, A., Abella, A., Marti, L., Carpéné, C., Palacín, M., and Testar, X. (2003) Semicarbazide-sensitive amine oxidase activity exerts insulin-like effects on glucose metabolism and insulin-signaling pathways in adipose cells. *Biochim. Biophys. Acta 1647*, 3–9.

(13) Boomsma, F., Hut, H., Bagghoe, U., van der Houwen, A., and van den Meiracker, A. (2005) Semicarbazide-sensitive amine oxidase (SSAO): From cell to circulation. *Med. Sci. Monit. 11*, RA122–RA126.

(14) Jaakkola, K. et al. (2000) et al. In vivo detection of vascular adhesion protein-1 in experimental infiammation. *Am. J. Pathol. 157*, 463–471.

(15) Koskinen, K., Vainio, P. J., Smith, D. J., Pihlavisto, M., Ylä-Herttuala, S., Jalkanen, S., and Salmi, M. (2004) Granulocyte transmigration through the endothelium is regulated by the oxidase activity of vascular adhesion protein-1 (VAP-1). *Blood 103*, 3388–3395.

(16) Salmi, M., Yegutkin, G. G., Lehvonen, R., Koskinen, K., Salminen, T., and Jalkanen, S. (2001) A cell surface amine oxidase directly controls lymphocyte migration. *Immunity 14*, 265–276.

(17) Merinen, M., Irjala, H., Salmi, M., Jaakkola, I., Hänninen, A., and Jalkanen, S. (2005) Vascular dhesion protein-1 is involved in both acute and chronic inflammation in the mouse. *Am. J. Pathol. 166*, 793–800.

(18) Bonder, C. S., Norman, M. U., Swain, M. G., Zbytnuik, L. D., Yamanouchi, J., Santamaria, P., Ajuebor, M., Salmi, M., Jalkanen, S., and Kubes, P. (2005) Rules of recruitment for Th1 and Th2 lymphocytes in inflamed liver: A role for alpha-4 integrin and vascular adhesion protein-1. *Immunity 23*, 153–163.

(19) Lalor, P. F., Edwards, S., McNab, G., Salmi, M., Jalkanen, S., and Adams, D. H. (2002) Vascular adhesion protein-1 mediates adhesion and transmigration of lymphocytes on human epatic endothelial cells. *J. Immunol. 169*, 983–992.

(20) Tohka, S., Laukkanen, M., Jalkanen, S., and Salmi, M. (2001) Vascular adhesion protein 1 (VAP-1) functions as a molecular brake during granulocyte rolling and mediates recruitment n vivo. *FASEB J. 15*, 373–382.

(21) Abella, A., Marti, L., Carpéné, C., Palacín, M., Testar, X., and Zorzano, A. (2003) Stimulation of glucose transport by semicarbazide-sensitive amine oxidase activity in adipocytes from diabetic rats. *J. Physiol. Biochem. 59*, 153–160.

(22) Kurkijärvi, R., Adams, D. H., Leino, R., Möttönen, T., Jalkanen, S., and Salmi, M. (1998) Circulating form of human vascular adhesion protein-1 (VAP-1): Increased serum levels in infiammatory liver diseases. *J. Immunol. 161*, 1549–1557.

(23) Stolen, C. M., Yegutkin, G. G., Kurkijärvi, R., Bono, P., Alitalo, K., and Jalkanen, S. (2004) Origins of serum semicarbazide-sensitive amine oxidase. *Circ. Res. 95*, 50–57.

(24) Yu, P. H., Wright, S., Fan, E. H., Lun, Z.-R., and Gubisne-Harberle, D. (2003) Physiological and pathological implications of semicarbazide-sensitive amine oxidase. *Biochim. Biophys. Acta 1647*, 193–199.

(25) Schwelberger, H. G. (2007) The origin of mammalian plasma amine oxidases. *J. Neural Transm. 114*, 757–762.

(26) Holt, A., Smith, D. J., Cendron, L., Zanotti, G., Rigo, A., and Di Paolo, M. L. (2008) Multiple binding sites for substrates and modulators of semicarbazide-sensitive amine oxidases: Kinetic consequences. *Mol. Pharmacol. 73*, 525–538.

(27) Airenne, T. T., Nymalm, Y., Kidron, H., Smith, D. J., Pihlavisto, M., Salmi, M., Jalkanen, S., Johnson, M. S., and Salminen, T. A. (2005) Crystal structure of the human vascular adhesion protein-1: Unique structural features with functional implications. *Protein Sci. 14*, 1964–1974.

(28) Jakobsson, E., Nilsson, J., Ogg, D., and Kleywegt, G. J. (2005) Structure of human semicarbazide-sensitive amine oxidase/vascular adhesion protein-1. *Acta Crystallogr. D61*, 1550–1562.

(29) McGrath, A. P., Hilmer, K. M., Collyer, C. A., Shepard, E. M., Elmore, B. O., Brown, D. E., Dooley, D. M., and Guss, J. M. (2009) Structure and inhibition of human diamine oxidase. *Biochemistry 48*, 9810–9822.

(30) Ernberg, K., McGrath, A., Peat, T., Adams, T., Xiao, X., Pham, T., Newman, J., McDonald, I., Collyer, C., and Guss, J. (2010) A new crystal form of human vascular adhesion protein 1. *Acta Crystallogr. F66*, 1572–1578.

(31) Smith, D. J., Salmi, M., Bono, P., Hellman, J., Leu, T., and Jalkanen, S. (1998) Cloning of vascular adhesion protein 1 reveals a novel multifunctional adhesion molecule. *J. Exp. Med. 188*, 17–27.

(32) Nymalm, Y., Kidron, H., Söderholm, A., Viitanen, L., Kaukonen, K., Pihlavisto, M., Smith, D. J., Veromaa, T., Airenne, T. T., Johnson, M. S., and Salminen, T. A. (2003) Crystallization and preliminary X-ray analysis of the human vascular adhesion protein-1. *Acta Crystallogr. D59*, 1288–1290.

(33) Salminen, T. A., Airenne, T., Johnson, M., Kidron, H., Nymalm, Y., Söderholm, A., Smith, D. J., Pihlavisto, M., Viitanen, L., Pentikäinen, O., and Nyrönen, T. (2004) Crystalline VAP-1 and uses thereof. WO 2004/104191.

(34) Kabsch, W. (1993) Automatic processing of rotation diffraction data from crystals of initially unknown symmetry and cell constants. *J. Appl. Crystallogr. 26*, 795–800.

(35) McCoy, A. J., Grosse-Kunstleve, R. W., Adams, P. D., Winn, M. D., Storoni, L. C., and Read, R. J. (2007) Phaser crystallographic software. *J. Appl. Crystallogr. 40*, 658–674.

(36) Collaborative Computational Project Number 4. (1994) The CCP4 suite: Programs for protein crystallography. *Acta Crystallogr. D50*, 760–763.

(37) Murshudov, G. N., Vagin, A. A., and Dodson, E. J. (1997) Refinement of macromolecular structures by the maximum-likelihood method. *Acta Crystallogr. D53*, 240–255.

(38) Emsley, P., and Cowtan, K. (2004) Coot: Model-building tools for molecular graphics. *Acta Crystallogr. D60*, 2126–2132.

(39) Adams, P. D. et al. (2010) et al. PHENIX: A comprehensive Python-based system for macromolecular structure solution. *Acta Crystallogr. D66*, 213–221.

(40) Terwilliger, T. C., Grosse-Kunstleve, R. W., Afonine, P. V., Moriarty, N. W., Adams, P. D., Read, R. J., Zwart, P. H., and Hung, L.-W. (2008) Iterative-build OMIT maps: Map improvement by iterative model building and refinement without model bias. *Acta Crystallogr. D64*, 515–524.

(41) Laskowski, R. A., MacArthur, M. W., Moss, D. S., and Thornton, J. M. (1993) PROCHECK: A program to check the stereochemical quality of protein structures. *J. Appl. Crystallogr. 26*, 283–291.

(42) Vriend, G. (1990) WHAT IF: A molecular modeling and drug design program. *J. Mol. Graphics 8* (52−56), 52–56, 29.

(43) Lowry, O. H., Rosebrough, N. J., Farr, A. L., and Randall, R. J. (1951) Protein measurement with the folin phenol reagent. *J. Biol. Chem. 193*, 265–275.

(44) Peterson, G. L. (1979) Review of the folin phenol protein quantitation method of Lowry, Rosebrough, Farr, and Randall. *Anal. Biochem. 100*, 201–220.

(45) Fowler, C., and Tipton, K. (1981) Concentration dependence of the oxidation of tyramine by the two forms of rat liver mitochondrial monoamine oxidase. *Biochem. Pharmacol. 30*, 3329–3332.

(46) Jaakkola, K., Kaunismäki, K., Tohka, S., Yegutkin, G., Vänttinen, E., Havia, T., Pelliniemi, L., Virolainen, M., Jalkanen, S., and Salmi, M. (1999) Human vascular adhesion protein-1 in smooth muscle cells. *Am. J. Pathol. 155*, 1953–1965.

(47) Jones, G., Willett, P., and Glen, R. C. (1995) Molecular recognition of receptor sites using a genetic algorithm with a description of desolvation. *J. Mol. Biol. 245*, 43–53.

(48) Jones, G., Willett, P., Glen, R. C., Leach, A. R., and Taylor, R. (1997) Development and validation of a genetic algorithm for flexible docking. *J. Mol. Biol. 267*, 727–748.

(49) Laskowski, R. A. (1995) SURFNET: A program for visualizing molecular surfaces, cavities, and intermolecular interactions. *J. Mol. Graphics 13*, 307–308, 323−330.

(50) DeLano, W. (2002) *PyMOL*, DeLano Scientific, San Carlos, CA.

(51) Johnson, M. S., and Overington, J. P. (1993) A structural basis for sequence comparisons. An evaluation of scoring methodologies. *J. Mol. Biol. 233*, 716–738.

(52) Lehtonen, J. V., Still, D. J., Rantanen, V. V., Ekholm, J., Bjorklund, D., Iftikhar, Z., Huhtala, M., Repo, S., Jussila, A., Jaakkola, J., Pentikainen, O., Nyronen, T., Salminen, T., Gyllenberg, M., and Johnson, M. S. (2004) BODIL: A molecular modeling environment for structure−function analysis and drug design. *J. Comput.-Aided Mol. Des. 18*, 401–419.

(53) Parsons, M. R., Convery, M. A., Wilmot, C. M., Yadav, K. D., Blakeley, V., Corner, A. S., Phillips, S. E., McPherson, M. J., and Knowles, P. F. (1995) Crystal structure of a quinoenzyme: Copper amine oxidase of *Escherichia coli* at 2 Å resolution. *Structure 3*, 1171–1184.

(54) Janes, S. M., Palcic, M. M., Scaman, C. H., Smith, A. J., Brown, D. E., Dooley, D. M., Mure, M., and Klinman, J. P. (1992) Identification of topaquinone and its consensus sequence in copper amine oxidases. *Biochemistry 31*, 12147–12154.

(55) Julenius, K., Mølgaard, A., Gupta, R., and Brunak, S. (2005) Prediction, conservation analysis, and structural characterization of mammalian mucin-type O-glycosylation sites. *Glycobiology 15*, 153–164.

(56) Li, R., Klinman, J. P., and Mathews, F. S. (1998) Copper amine oxidase from *Hansenula polymorpha*: The crystal structure determined at 2.4 Å resolution reveals the active conformation. *Structure 6*, 293–307.

(57) McGrath, A., Hilmer, K., Collyer, C., Dooley, D., and Guss, J. (2010) A new crystal form of human diamine oxidase. *Acta Crystallogr. F66*, 137–142.

(58) Duff, A. P., Trambaiolo, D. M., Cohen, A. E., Ellis, P. J., Juda, G. A., Shepard, E. M., Langley, D. B., Dooley, D. M., and Freeman, H. C. (2004) Using xenon as a probe for dioxygenbinding sites in copper amine oxidases. *J. Mol. Biol. 344*, 599–607.

(59) Duff, A., Cohen, A., Ellis, P., Hilmer, K., Langley, D., Dooley, D., Freeman, H., and Guss, J. (2006) The 1.23 Angstrom structure of *Pichia pastoris* lysyl oxidase reveals a lysine-lysine cross-link. *Acta Crystallogr. D62*, 1073–1084.

(60) Kelly, I. D., Knowles, P. F., Yadav, K. D., Bardsley, W. G., Leff, P., and Waight, R. D. (1981) Steady-state kinetic studies on benzylamine oxidase from pig plasma. *Eur. J. Biochem. 114*, 133–138.

(61) Zhang, Y., Ran, C., Zhou, G., and Sayre, L. (2007) Highly potent 3-pyrroline mechanismbased inhibitors of bovine plasma amine oxidase and mass spectrometric confirmation of cofactor derivatization. *Bioorg. Med. Chem. 15*, 1868–1877.

(62) Chang, C., Klema, V., Johnson, B., Mure, M., Klinman, J., and Wilmot, C. (2010) Kinetic and structural analysis of substrate specificity in two copper amine oxidases from *Hansenula polymorpha*. *Biochemistry 49*, 2540–2550.

(63) Holt, A., Wieland, B., and Baker, G. B. (2004) Allosteric modulation of semicarbazide sensitive amine oxidase activities in vitro by imidazoline receptor ligands. *Br. J. Pharmacol. 143*, 495–507.

(64) Farnum, M., Palcic, M., and Klinman, J. P. (1986) pH dependence of deuterium isotope effects and tritium exchange in the bovine plasma amine oxidase reaction: A role for single-base catalysis in amine oxidation and imine exchange. *Biochemistry 25*, 1898–1904.

(65) Su, Q., and Klinman, J. P. (1998) Probing the mechanism of proton coupled electron transfer to dioxygen: The oxidative half-reaction of bovine serum amine oxidase. *Biochemistry 37*, 12513–12525.

(66) Lunelli, M., Di Paolo, M. L., Biadene, M., Calderone, V., Battistutta, R., Scarpa, M., Rigo, A., and Zanotti, G. (2005) Crystal structure of amine oxidase from bovine serum. *J. Mol. Biol. 346*, 991–1004.

(67) Nurminen, E. M., Pihlavisto, M., Lázár, L., Szakonyi, Z., Pentikäinen, U., Fülöp, F., and Pentikäinen, O. (2010) Synthesis, in vitro activity, and three-dimensional quantitative structure-activity relationship of novel hydrazine inhibitors of human vascular adhesion protein-1. *J. Med. Chem. 53*, 6301–6315.

(68) Duff, A. P., Cohen, A. E., Ellis, P. J., Kuchar, J. A., Langley, D. B., Shepard, E. M., Dooley, D. M., Freeman, H. C., and Guss, J. M. (2003) The crystal structure of *Pichia pastoris* lysyl oxidase. *Biochemistry 42*, 15148–15157.

(69) Wilmot, C. M., Murray, J. M., Alton, G., Parsons, M. R., Convery, M. A., Blakeley, V., Corner, A. S., Palcic, M. M., Knowles, P. F., McPherson, M. J., and Phillips, S. E. (1997) Catalytic mechanism of the quinoenzyme amine oxidase from *Escherichia coli*: Exploring the reductive half-reaction. *Biochemistry 36*, 1608–1620.